# An LMI-based discrete time nonlinear observer for Light-Emitting Diode optical communication

Automatica 141 (2022) 110309

Contents lists available at ScienceDirect

Automatica

journal homepage: www.elsevier.com/locate/automatica

# An LMI-based discrete time nonlinear observer for Light-Emitting Diode optical communication ☆

Ibrahima N'Doye [a,1], Ding Zhang [b,1], Ania Adil [a], Ali Zemouche [c,e], Rajesh Rajamani [d], Taous-Meriem Laleg-Kirati [a,*]

[a] Computer, Electrical and Mathematical Sciences and Engineering Division (CEMSE), King Abdullah University of Science and Technology (KAUST), Thuwal 23955-6900, Saudi Arabia
[b] Department of Electronic and Computer Engineering, The Hong Kong University of Science and Technology, Clear Water Bay, Kowloon, Hong Kong, China
[c] University of Lorraine, CRAN CNRS UMR 7039, 54400 Cosnes et Romain, France
[d] Department of Mechanical Engineering, University of Minnesota, MN 55455, USA
[e] EPI-DISCO (external collaborator), Inria-Saclay, Gif-sur-Yvette, France

ARTICLE INFO

*Article history:*
Received 2 March 2021
Received in revised form 11 December 2021
Accepted 2 February 2022
Available online xxxx

*Keywords:*
Optical wireless communication
Light-emitting diode (LED) optical communication
Nonlinear observer design
Monotonic systems
Switched systems
Linear matrix inequality (LMI) approach

ABSTRACT

Light-Emitting Diode (LED) optical wireless communication is a potentially low-cost, sustainable approach for enabling high-speed free-space and underwater transmissions within a limited communication range. Establishing a tightly controlled line of sight (LOS) between transmitter and receiver is a significant challenge because the angle of the alignment is not directly measured and has to be estimated. To address this problem, we propose a novel switched-gain discrete-time nonlinear observer for an LED-based optical communication model in which the nonlinear output functions are composed of nonlinear vector functions of multi-scalar combinations of the states. Lyapunov function-based analysis that ensures global stability is used to design the proposed observer in each piecewise monotonic region of the LED output functions. Furthermore, we prove via a quadratic Lyapunov-based approach that a constant stabilizing observer gain design approach has no feasible solution when the entire LED optical communication range is considered. Therefore, a suitable switched-gain nonlinear observer is derived for non-monotonic output measurement equations. Simulation results are shown together with extensive comparisons with the Extended Kalman Filter (EKF) to illustrate the performance of the proposed switched-gain observer design.



## 1. Introduction

Many research efforts are devoted to advancing Optical Wireless Communication (OWC) technology for indoor and outdoor applications as the demand for capacity increases. OWC is considered an emerging alternative technology in the communication area. It carries out flexible networking solutions with cost-effective and high-speed license-free wireless connectivity for several applications (Ghassemlooy et al., 2012; N'Doye et al., 2018; Zhang et al., 2020). Compared to radio-frequency (RF) and acoustic communication systems, OWC technology provides low latency, low cost and power consumption, and high data rates (Hagem et al., 2011; Hanson & Radic, 2008; Lu et al., 2009).

Most communication for above-ground robots and devices occurs through RF communication. RF communication has been the standard method for the autonomous ground robotic network to operate wirelessly. However, RF technology presents limitations such as a limited available data rate and congested spectrum (Borah et al., 2012; Ghassemlooy et al., 2012). Hence, optical wireless communication (OWC) technology is an alternative that can complement RF technology to overcome these limitations (Borah et al., 2012; Elgala et al., 2011; Ghassemlooy et al., 2012; Majumdar & Ricklin, 2010). The practical applications of the free-space optical communication system have been a great interest of wide field-of-view (FoV) such that NASA technologies for interplanetary free-space optical (FSO) communication systems, Facebook drones Aquila (Nov, 2018), Google's internet balloons (De-Vaul

☆ This work has been supported by the King Abdullah University of Science and Technology (KAUST) through Base Research Fund (BAS/1/1627-01-01). The 21st IFAC World Congress (IFAC 2020), July 12–17, 2020, Berlin, Germany. This paper was recommended for publication in revised form by Associate Editor Angelo Alessandri under the direction of Editor Thomas Parisini.

* Corresponding author.
*E-mail addresses:* ibrahima.ndoye@kaust.edu.sa (I. N'Doye), ding.zhang@connect.ust.hk (D. Zhang), ania.adil@kaust.edu.sa (A. Adil), ali.zemouche@univ-lorraine.fr (A. Zemouche), rajamani@me.umn.edu (R. Rajamani), taousmeriem.laleg@kaust.edu.sa (T.-M. Laleg-Kirati).

[1] The two first authors contributed equally to the paper

https://doi.org/10.1016/j.automatica.2022.110309

et al., 2014), FSO communication in space (Elgala et al., 2017), and military platforms (Soo Sim Daniel, 2003).

Furthermore, the rapid adaption and decreasing cost of the light-emitting-diode (LED) makes it a compelling alternative and a promising communication technique to acoustic and radio-based wireless free-space and underwater optical communications (N'Doye et al., 2020; Zhang et al., 2020). Although there is extensive effort to build reliable OWC for mobile networking sensing applications, however, OWC systems' practicality to maintain accurate alignment angle of tracking optical systems in autonomous robot platforms has been, until recently, a significant problem. In addition, the required alignment angle is not directly measured and has to be estimated.

Kalman-type filters have been considered industry-standard solutions for motion control problems and navigation systems. However, these filters rely on local linearization assumptions and fail when the initial estimation errors are large. Furthermore, previous results on the Extended Kalman Filter (EKF)-based algorithm of maintaining active alignment control for LED-based wireless optical communications lack strong theoretical stability guarantees of the convergence of the estimator (Solanki et al., 2016, 2018). Indeed, small errors in the output measurement can make the EKF system go unstable.

Recently, some interesting results based on the moving horizon estimation (MHE) algorithm for robot vehicle position problem have been addressed in Alessandri and Gaggero (2019) and Alessandri et al. (2019). MHE can handle constraints in a consistent manner and varying measurement delays. However, the increased computational requirements for MHE over a long estimation horizon might lead to an intractable infinite-horizon estimation problem in practical applications (Rolf et al., 2007), despite the recent attempts to reduce the computational burden (Alessandri & Gaggero, 2019). On the other hand, sliding-mode (SM) estimator and high-order SM observers may provide higher performance than an EKF (Alessandri, 2003). However, these observers have complex design conditions and lack robustness (Rajamani et al., 2017).

In contrast to the moving horizon estimation and sliding mode observer frameworks, LMI-based observer design techniques have been widely used for different classes of nonlinear systems (Acikmese & Corless, 2011; Arcak & Kokotovic, 2001; Draa et al., 2019; Ha & Trinh, 2004; Wang et al., 2014; Zemouche et al., 2017). Moreover, these developed LMI-based observer design methods in the literature may fail when it comes to actual application to non-monotonic nonlinear systems (Rajamani et al., 2020). On the other hand, the authors in Lacerda et al. (2014) and Li et al. (2012) proposed filters for polynomial systems with $\mathcal{H}_\infty$ performance. A nice feature of these filters is that they rely on Sum-of-Square (SOS) approaches and quadratic Lyapunov functions. Indeed, the SOS techniques may overcome infeasibility problems on the LMI-based filter design since a general Lyapunov function with additional decision variables may modify the structure of the LMI avoiding infeasibility in the case of non-monotonicity of the nonlinear output functions.

Recently, a novel LMI-based switched-gain observer design method for nonlinear continuous systems has been nicely developed in Rajamani's work (Rajamani et al., 2020) to tackle the non-monotonicity gap. The developed algorithm works effectively when the involved nonlinear functions are non-monotonic and depend on scalar variables. However, it fails when the involved nonlinear non-monotonic output functions depend on an arbitrary number of multi-dimensional variables. Indeed, the method in Rajamani et al. (2020) needs to be extended to discrete-time systems and to be generalized to systems in which the output nonlinearities depend on multi-dimensional variables. Hence, we propose a discrete-time nonlinear switched-gain observer for the LED-based optical communication system. The LED model's output functions are involved in nonlinear vector functions of multi-scalar combinations of the states.

In this present work, we propose a scenario in which mobile vehicle robotic agents are used for mobile networking sensing applications. Our research aims at designing a discrete-time nonlinear switched-gain observer for nonlinear output equations to estimate the angle between the receiver aperture and the LOS beam sent by the transmitter for an LED-based optical communication system. For each piecewise monotonic region, we derive a constant stabilizing observer gain to ensure global asymptotic stability. The proposed observer experiences switched gains when a measurement is available in each region, then the whole updated process error dynamics is described as a switched-gain system. The benefit of the proposed switched-gain nonlinear observer is its efficiency in guaranteeing global asymptotic stability compared to the stochastic filters.

Note that a preliminary version of this work appeared as a conference paper in N'Doye et al. (2020). In this extended version, we

- provide complete proofs of the main results,
- derive a general synthesis method for an asymptotic convergence of the estimation error for monotonic systems,
- demonstrate the infeasibility to solutions for the observer design LMIs when the nonlinear functions are all non-monotonic,
- conduct detailed simulation results to analyze the capability of the proposed switched-gain observer design approach to reconstruct the states in comparison to the standard extended Kalman filter (EKF).

The outline of the rest of the paper is as follows. In Section 2, the optical channel modeling of the LED system is presented, including the luminous flux model and its state–space formulation. In Section 3, we formulate our estimation problem. Then, we provide details about the asymptotic convergence of the estimation error, the demonstration of infeasibility to solutions for the observer design LMIs when the nonlinear LED functions are all non-monotonic, and the application of the developed switched-gain observer techniques for LED-based optical communication. In Section 4, simulation results are illustrated to compare the performance of the proposed switched-gain observer and EKF. Finally, concluding remarks are shown in Section 5.

**Notation:** Matrix $A^\top$ represents the transposed matrix of $A$. The Euclidean norm of a vector $x \in \mathbb{R}^n$ is defined as $\|x\| = \sqrt{x^\top x}$. The identity matrix of dimension $r$ is denoted $\mathbb{I}_r$. The blocks induced by symmetry are denoted $(\star)$. The set $Co(x, y) = \{\lambda x + (1-\lambda)y,\ 0 \leqslant \lambda \leqslant 1\}$ is the convex hull of $\{x, y\}$. A vector of the canonical basis of $\mathbb{R}^s$ is denoted $e_s(i) = \big(0, \ldots, 0, \overbrace{1}^{i\text{th}}, 0, \ldots, 0\big)^\top \in \mathbb{R}^s$, $s \geqslant 1$. ($s$ components). A positive definite (negative definite) square matrix is denoted $S > 0$ ($S < 0$). $\mathbb{N}_+$ is the set of positive integers.

## 2. LED-based optical channel modeling

The LED-based optical channel describes a two-way communication that consists of an LED transmitter and a photodiode receiver; each end can rotate by an angle in which it establishes and maintains LOS. Fig. 1 illustrates the experimental setup for an estimation problem of LED-based optical channel modeling.


**Fig. 1.** Mobile networking of ground vehicle robots with LED-based communication.

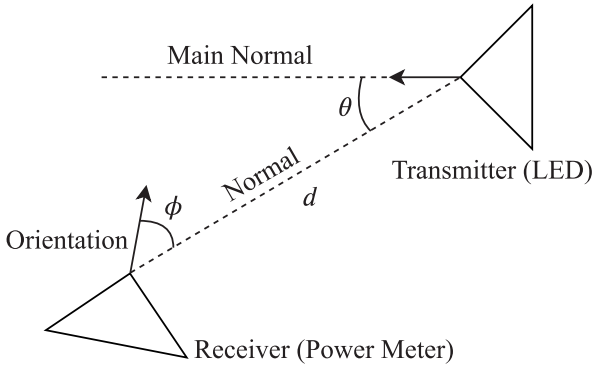


**Fig. 2.** LED communication scheme.

### 2.1. LED-based intensity model

The detector's incident power can be determined based on the signal irradiance at the relative detector position. Fig. 2 illustrates the variables of interest, which include the transmission distance $d$, the transmission angle $\theta$, and the angle of incidence of $\phi$.

The full signal strength model can be formulated as follows (Doniec et al., 2013; Ghassemlooy et al., 2012; Solanki et al., 2016, 2018)

$$P_d = CI(\theta, d)\exp(-cd)g(\phi), \tag{1}$$

where $P_d$ is the measurement of power, which is proportional to the luminous flux of light detected by the receiver, $C$ and $c$ are both constants. The $\exp(-cd)$ portion comes from Beer–Lambert's law (Miller et al., 2009) which describes the attenuation of power when light travels through medium as an exponential decay; $I(\theta, d)$ is usually in the following form (Doniec et al., 2013; Ghassemlooy et al., 2012; Solanki et al., 2016, 2018)

$$I(\theta, d) = I(0, d)\cos^m(\theta)/d^2, \tag{2}$$

where $I(0)$ is the central luminous flux, as well as the maximum luminous flux, and $m$ is the order of Lambertian emission

$$m = \frac{\ln(2)}{\ln\cos(\theta_{1/2})}.$$

In the above formula, $\theta_{1/2}$ is the angle at half the illuminance of an LED. Physically, $I(0, d)\cos^m(\theta)$ represents the radiation pattern of LED source (Ivan & Ching-Cherng, 2008) and the reciprocal of $d^2$ comes from the inverse-square law, which describes the geometric dilution of a physical quantity. The resulting luminous flux model is given as follows (N'Doye et al., 2020).

$$P_d(d, \theta, \phi) = \underbrace{\frac{a\exp(-bd)}{d^2}\tilde{I}_\theta}_{\text{Transmitter}}\ \underbrace{g(\phi)}_{\text{Receiver}}, \tag{3}$$

where $\tilde{I}_\theta$ is the angular intensity distribution of the transmitter, $g(\phi)$ is the dependence of the received LED intensity on the incidence angle $\phi$ and takes the form of two Gaussian terms with six unknowns (N'Doye et al., 2020)

$$g(\phi) \approx a_1\exp\left[-\left(\frac{\phi - b_1}{c_1}\right)^2\right] + a_2\exp\left[-\left(\frac{\phi - b_2}{c_2}\right)^2\right]. \tag{4}$$

All the constants values in this section are nonnegative, and their physical meaning can be found in Table 1.

### 2.2. State–space formulation

We note that, in practice, it is not easy to move the distance $d$ desirably because it requires moving the whole robot platform. From (3), we formulate the state space equation through the three variables of interest: the angular transmission intensity distribution $\tilde{I}_\theta$, the angular position of the receiver $\phi$, and the angular velocity of the receiver $\dot{\phi}$. Subsequently, controlling the angular velocity $\dot{\phi}$ is more independent and involves a local decision in practice. The aim consists of adjusting the angular velocity $\dot{\phi}$ to zero, which acts to the angular position $\phi$ to get alignment for both robots on each side of communication. We combine $\tilde{I}_\theta$ and $d$ in one state variable ($x_1 = f(d, \tilde{I}_\theta)$) as we mentioned before that $d$ cannot be adjusted easily. Therefore, we define the states as follows

$$x = \begin{bmatrix} x_1 \\ x_2 \\ x_3 \end{bmatrix} = \begin{bmatrix} C_p\tilde{I}_\theta\exp(-cd)/d^2 \\ \phi \\ \dot{\phi} \end{bmatrix}, \tag{5}$$

where $\phi \triangleq x_2$ is the angular position and $\dot{\phi} \triangleq x_3$ is the angular velocity.

Here, the state variables of the moving LED in time fall into the following form

$$\begin{bmatrix} x_1(t+\Delta t) \\ x_2(t+\Delta t) \\ x_3(t+\Delta t) \end{bmatrix} = \begin{bmatrix} x_1(t) \\ x_2(t) + x_3(t)\Delta t \\ x_3(t) \end{bmatrix}. \tag{6}$$

The discrete-time state space representation can be written as follows

$$x_k = \begin{bmatrix} x_{1,k} \\ x_{2,k} \\ x_{3,k} \end{bmatrix} = \begin{bmatrix} x_{1,k-1} + w_{1,k-1} \\ x_{2,k-1} + T_e x_{3,k-1} + w_{2,k-1} \\ x_{3,k-1} + u_{k-1} + w_{3,k-1} \end{bmatrix}, \tag{7}$$

in which the states $x_2$ and $x_3$ are sampled synchronously at the sampling time $T_e = k\Delta t$ by the time index $k$. $w_{1,k}$, $w_{2,k}$ and $w_{3,k} \in \ell_2$ are the process noises which are assumed to be Gaussian, independent and white. $u_k$ is the control input which acts on the receiver angular velocity.

### 2.3. Output measurement equation

The measurement $P_{d,k}$ is expressed as

$$y_k \triangleq P_{d,k} = x_{1,k}g(x_{2,k}) + v_k, \tag{8}$$

where $g(.)$ is defined in (4) and $v_k \in \ell_2$ is an additive white Gaussian noise.

The system is locally unobservable at $\phi = 0°$. Hence, we introduce a second receiver on the same robot. Then, we place each receiver symmetrically with fixed shifted angle $\Delta\phi_1 = 6°$ and $\Delta\phi_2 = -6°$ to achieve observability, as illustrated in Fig. 3. These shifted angles are added to account for the receiver's actual angular position orientation. At each movement of the transmitter platform, the states are updated according to the system dynamics. When $\phi_1$ is controlled to 0° and reads the wireless

**Table 1**
LED parameters value.

| Terms | Model | Parameters | | | | | | $R^2$ | RMSE |
|---|---|---|---|---|---|---|---|---|---|
| | | $a(a_1)$ | $b(b_1)$ | $c(c_1)$ | $a_2$ | $b_2$ | $c_2$ | | |
| Scattering, absorption, dilution | $a\exp(-bx)/x^2$ | 0.01009 | 1.972 | – | – | – | – | 0.9947 | 0.0058 |
| Receiver orientation | $a_1\exp\left[-\left(\frac{x-b_1}{c_1}\right)^2\right]+a_2\exp\left[-\left(\frac{x-b_2}{c_2}\right)^2\right]$ | 0.9953 | 0.06298 | 0.2517 | 0.2260 | −0.1995 | 0.132 | 0.9970 | 0.0205 |

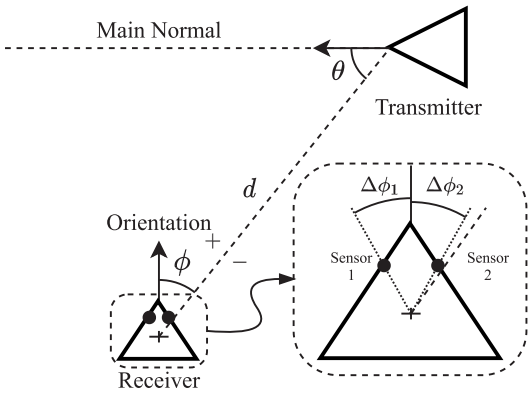


**Fig. 3.** Measurements of two receivers $\phi_1$ and $\phi_2$.

transmitted data, its orientation is being maintained by using $\phi_2$. Hence, the resulting output vector can be written as follows

$$\begin{bmatrix} y_{1,k} \\ y_{2,k} \end{bmatrix} = \begin{bmatrix} x_{1,k} g(\overbrace{x_{2,k} + \Delta\phi_1}^{\phi_1}) \\ x_{1,k} g(\underbrace{x_{2,k} + \Delta\phi_2}_{\phi_2}) \end{bmatrix} + v_k. \tag{9}$$

Given the measurement, the primary goal is to estimate $x_{1,k}$, the angular position $\phi \triangleq x_{2,k}$ and the angular velocity $\dot{\phi} \triangleq x_{3,k}$ based on which the control $u_k$ is designed, to drive $x_{3,k}$ and indirectly $x_{2,k}$ towards zero, which corresponds to the maximum light intensity's orientation.

The next section is devoted to a general theory providing a general observer design method, which can be used for other real-world applications.

## 3. A general observer design theory

This section is devoted to a general theory on state observer design. This theory is motivated by the LED-based optical communication model described in (7) and (9).

### 3.1. Problem formulation

In this paper, we consider the family of linear systems with nonlinear output measurements, described by the following set of equations

$$\begin{cases} x_{k+1} = Ax_k + Bu_k + Ew_k \\ y_k = h(x_k) + Dw_k \end{cases} \tag{10}$$

where $x_k \in \mathbb{R}^n$ is the state vector, $u_k \in \mathbb{R}^m$ is the input vector, $y_k \in \mathbb{R}^p$ is the output measurement, $w_k \in \mathbb{R}^z$ is the disturbance $\ell_2$ bounded vector and the matrices $A \in \mathbb{R}^{n\times n}$, $B \in \mathbb{R}^{n\times m}$, $E \in \mathbb{R}^{n\times z}$ and $D \in \mathbb{R}^{p\times z}$ are constant. The nonlinear output function $h: \mathbb{R}^n \longrightarrow \mathbb{R}^p$ is assumed to be globally Lipschitz.

To estimate the unmeasurable state variables of the model (10), we propose the following nonlinear observer structure

$$\hat{x}_{k+1} = A\hat{x}_k + Bu_k + L\Big(y_k - h(\hat{x}_k)\Big), \tag{11}$$

where $\hat{x}_k$ is the estimate of $x_k$. The matrix $L \in \mathbb{R}^{n\times p}$ is the observer gain parameter to be determined later. Since $h(.)$ is globally Lipschitz, then, there exist $z_i \in Co(\vartheta_i, \hat{\vartheta}_i)$, functions $\phi_{ij}: \mathbb{R}^{n_i} \longrightarrow \mathbb{R}$, and constants $a_{ij}$, $b_{ij}$, such that

$$h(x) - h(\hat{x}) = \sum_{i,j=1}^{p,n_i} \phi_{ij}(z_i)\mathcal{H}_{ij}\Big(\vartheta_i - \hat{\vartheta}_i\Big), \tag{12}$$

and

$$\vartheta_i = H_i x_k, \quad \hat{\vartheta}_i = H_i\hat{x}_k,$$
$$a_{ij} \leqslant \phi_{ij}\Big(z_i\Big) \leqslant b_{ij}, \quad \phi_{ij}(z_i) = \frac{\partial h_i}{\partial \vartheta_i^j}(z_i), \tag{13}$$

where

$$\mathcal{H}_{ij} = e_p(i)e_{n_i}^{\top}(j), \quad \phi_{ij} \triangleq \phi_{ij}\Big(z_i\Big), \quad H_i \in \mathbb{R}^{n_i\times n}.$$

Since $\vartheta_i - \hat{\vartheta}_i = H_i e_k$ and for all $i = 1, \ldots, p$ and $j = 1, \ldots, n_i$, we can rewrite the nonlinearities as follows

$$h(x_k) - h(\hat{x}_k) = \sum_{i,j=1}^{p,n_i} \phi_{ij}\mathcal{H}_{ij}H_i e_k \triangleq Ce_k + \sum_{i,j=1}^{p,n_i} \tilde{\phi}_{ij}\mathcal{H}_{ij}H_i e_k,$$

where

$$C \triangleq \sum_{(i,j)\in\mathfrak{F}} a_{ij}\mathcal{H}_{ij}H_i,$$
$$\tilde{\phi}_{ij} \triangleq \phi_{ij} - a_{ij}, \ \mathfrak{F} \triangleq \Big\{(i,j) : a_{ij} \neq 0\Big\}. \tag{14}$$

By definition, the matrix $C$ contains the quantities $a_{ij} \neq 0$. Then when all the nonlinearities are non-monotonic, the matrix $C$ will contain ALL the quantities $a_{ij}$ of the system.

Then, the dynamic equation of the observation error $e_k = x_k - \hat{x}_k$ can be written as

$$\begin{aligned} e_{k+1} &= \left(A - L\sum_{i,j=1}^{p,n_i}\Big[\phi_{ij}\mathcal{H}_{ij}H_i\Big]\right)e_k + \underbrace{\Big(E - LD\Big)}_{\mathbb{E}} w_k \\ &= \underbrace{\left(A - LC - \sum_{i,j=1}^{p,n_i}\tilde{\phi}_{ij}L\mathcal{H}_{ij}H_i\right)}_{\mathbb{A}} e_k + \mathbb{E}w_k. \end{aligned} \tag{15}$$

It follows that

$$0 \leqslant \tilde{\phi}_{ij} \leqslant \tilde{b}_{ij} \triangleq b_{ij} - a_{ij}.$$

**Remark 1.** Note that matrix $H_i$ is a linear transformation mapping from the state variable to a vector of new variables which the $i$th component of output function depends on. In general, we look at the output function, which is vector-valued, in a component-wise way. Then, each component of the output function is a multivariate scalar-valued nonlinear function. These nonlinear functions, if analytic, can be written as a compound of transcendental functions which depend on the state variables. Whenever the state variables appear as a linear combination (including the case where a standalone state variable appears), we rename this

linear combination to a new variable. Then $H_i$ is a mapping from the original set of state variables to the set of these new variables. For example, assume the state $x = \begin{bmatrix} x_1 & x_2 & x_3 \end{bmatrix}^\top \in \mathbb{R}^3$ and the $i$th component of the output function $y_i = x_1 e^{x_2+x_3}$. In this case, $y_i$ depends on $\vartheta_1 = x_1$ and $\vartheta_2 = x_2 + x_3$, i.e., $y_i = f_i(x_1, x_2 + x_3) = f_i\left(\begin{bmatrix} 1 & 0 & 0 \\ 0 & 1 & 1 \end{bmatrix} x\right)$. Therefore, $H_i = \begin{bmatrix} 1 & 0 & 0 \\ 0 & 1 & 1 \end{bmatrix}$.

Before introducing the design method, the following definition of $\mathcal{H}_\infty$ stability is used in the paper.

**Definition 1.** System (15) is $\mathcal{H}_\infty$ stable if there exist a positive scalar $\mu$ and a $\mathcal{K}_\infty-$function $\beta(.)$ such that

$$\|e\|_{\ell_2^n} \leqslant \sqrt{\mu \|w\|_{\ell_2^z}^2 + [\beta(\|e_0\|)]^2} \tag{16}$$

for any $\ell_2$ disturbance $w_k$ and any initial error $e_0$. The quantity $\sqrt{\mu}$ is called the disturbance attenuation level.

Definition 1 gives a more general $\mathcal{H}_\infty$ criterion than the standard one used in control problem. However, criterion (16) is itself a special case of a more general property, called Input-to-State-Stability (ISS). For more details, we refer the reader to Sontag (1989) and Sontag and Wang (1996).

The criterion (16) implies that the classical $\mathcal{H}_\infty$ performance indicator holds (Li & Fu, 1997). That is the transfer $\mathbb{T}_{ew}$ from $w$ to $e$ satisfies the $\mathcal{H}_\infty$ norm:

$$\|\mathbb{T}_{ew}\|_\infty \triangleq \sup_w \frac{\|e\|_{\ell_2^n}}{\|w\|_{\ell_2^z}} \leqslant \sqrt{\mu}, \quad e_0 = 0. \tag{17}$$

As usually, to perform the $\mathcal{H}_\infty$ analysis leading to the criterion (16), we use Lyapunov characterizations. The following lemma provides some particular sufficient conditions ensuring (16).

**Lemma 1.** *Assume there exist a Lyapunov function $V(.)$ and two $\mathcal{K}_\infty-$functions $\alpha(.)$ and $\beta(.)$ such that*

$$[\alpha(\|e_k\|)]^2 \leqslant V(e_k) \leqslant [\beta(\|e_k\|)]^2, \ \forall\, k \geqslant 0, \tag{18a}$$

$$\mathcal{W}_k \triangleq \Delta V_k + \|e_k\|^2 - \mu \|w_k\|^2 < 0, \ \forall\, e_k \not\equiv 0, w_k \in \ell_2, \tag{18b}$$

*where $\Delta V_k \triangleq V(e_{k+1}) - V(e_k)$. Then the criterion (16) holds.*

**Proof.** From inequality (18b), we have

$$V_{k+1} - V_k + \|e_k\|^2 \leqslant \mu \|w_k\|^2.$$

It follows that

$$\sum_{k=0}^{N} \Big(V_{k+1} - V_k\Big) + \sum_{k=0}^{N} \|e_k\|^2 \leqslant \mu \sum_{k=0}^{N} \|w_k\|^2,$$

which is identical to

$$V_N - V_0 + \sum_{k=0}^{N} \|e_k\|^2 \leqslant \mu \sum_{k=0}^{N} \|w_k\|^2.$$

Since from (18a), we have $V_N \geqslant [\alpha(\|e_N\|)]^2 > 0$ for $e_N \not\equiv 0$, then

$$\sum_{k=0}^{N} \|e_k\|^2 \leqslant \mu \sum_{k=0}^{N} \|w_k\|^2 + V_0,$$

which is equivalent

$$\lim_{N\to\infty} \sum_{k=0}^{N} \|e_k\|^2 \leqslant \mu \lim_{N\to\infty} \sum_{k=0}^{N} \|w_k\|^2 + V_0.$$

Also, from (18a), we have $V_0 \leqslant [\beta(\|e_0\|)]^2$. Consequently, we get

$$\|e\|_{\ell_2^n}^2 \leqslant \mu \|w\|_{\ell_2^z}^2 + V_0 \leqslant \mu \|w\|_{\ell_2^z}^2 + [\beta(\|e_0\|)]^2,$$

which is equivalent to (16).

In the sequel, in the LMI framework, we particularly use a standard quadratic Lyapunov function

$$V_k \triangleq V(e_k) = e_k^\top P e_k,$$

where $P = P^\top > 0$. In this case, inequality (18a) is satisfied with $\beta(\|e_k\|) = \sqrt{\lambda_{\max}(P)}\|e_k\|$. Hence, the aim consists in finding the observer gain $L$ and a Lyapunov matrix $P = P^\top > 0$ such that the following particular criterion holds:

$$\|e\|_{\ell_2^n} \leqslant \sqrt{\mu \|w\|_{\ell_2^z}^2 + \nu \|e_0\|^2} \tag{19}$$

where $\sqrt{\mu}$ is the disturbance attenuation level; $\mu$ is a free solution of a specific LMI condition to be established later, and $\nu = \lambda_{\max}(P)$.

Minimization of the upper bound $\mu$ of the $\mathcal{H}_\infty$ performance criterion (19) reflects the disturbance attenuation/rejection capability of the proposed observer against both the process and measurement noise, concatenated in a single vector $w_k$.

### 3.2. A general observer design method

This subsection will derive the theoretical results on the observer design procedure for a class of nonlinear monotonic output equations systems. We demonstrate infeasibility to solutions for the observer design LMIs when the nonlinear LED functions are all non-monotonic. Then, we present a switched-gain observer design methodology that enables stable observers for the non-monotonic output functions of the LED optical communication systems through an $\mathcal{H}_\infty$ filter with ensured disturbance level $\mu$.

The following theorem provides the conditions that guarantee the asymptotic stability of the estimation error system (15) in the $\mathcal{H}_\infty$-optimality sense (19).

**Theorem 1.** *Assume that there exist symmetric positive definite matrices $P \in \mathbb{R}^{n\times n}$, $\mathbb{S}_{ij} \in \mathbb{R}^{n_i \times n_i}$, $i = 1, \ldots, n$ and matrix $\mathcal{X} \in \mathbb{R}^{p\times n}$, so that the following LMI condition holds*

$$\min(\mu) \text{ subject to (21)} \tag{20}$$

$$\Sigma = \begin{bmatrix} \mathbb{M} & \begin{bmatrix} \Pi_1^\top & \ldots & \Pi_p^\top \end{bmatrix} \\ (\star) & -\Lambda \mathbb{N} \end{bmatrix} < 0, \tag{21}$$

*where*

$$\mathbb{M} = \begin{bmatrix} -P + \mathbb{I}_n & 0 & A^\top P - C^\top \mathcal{X} \\ (\star) & -\mu \mathbb{I}_z & E^\top P - D^\top \mathcal{X} \\ (\star) & (\star) & -P \end{bmatrix}, \tag{22}$$

$$\Pi_i = \begin{bmatrix} \Pi_{i1}^\top(\mathcal{X}, \mathbb{S}_{i1}) \ldots \Pi_{in_i}^\top(\mathcal{X}, \mathbb{S}_{in_i}) \end{bmatrix}^\top,$$

$$\Pi_{ij}^\top(\mathcal{X}, \mathbb{S}_{ij}) = \begin{bmatrix} 0 \\ 0 \\ -\mathcal{X}^\top \mathcal{H}_{ij} \end{bmatrix} + \begin{bmatrix} H_i^\top \\ 0 \\ 0 \end{bmatrix} \mathbb{S}_{ij}, \tag{23}$$

$$\Lambda = \textit{block-diag}\Big(\Lambda_1, \ldots, \Lambda_p\Big), \tag{24}$$

$$\Lambda_i = \textit{block-diag}\left(\frac{2}{\tilde{b}_{i1}}\mathbb{I}_{n_i}, \ldots, \frac{2}{\tilde{b}_{in_i}}\mathbb{I}_{n_i}\right), \tag{25}$$

$$\mathbb{N} = \textit{block-diag}\Big(\mathbb{N}_1, \ldots, \mathbb{N}_p\Big), \tag{26}$$

$$
\begin{aligned}
\mathcal{W}_k = e_k^\top & \left[ \left( A - LC - L \sum_{i,j=1}^{p,n_i} \left[ \tilde{\phi}_{ij} \mathcal{H}_{ij} H_i \right] \right)^\top P \left( A - LC - L \sum_{i,j=1}^{p,n_i} \left[ \tilde{\phi}_{ij} \mathcal{H}_{ij} H_i \right] \right) - P + \mathbb{I} \right] e_k \\
& + w_k^\top \left[ \left( E - LD \right)^\top P \left( E - LD \right) - \mu \mathbb{I} \right] w_k \\
& + e_k^\top \left[ \left( A - LC - L \sum_{i,j=1}^{p,n_i} \left[ \tilde{\phi}_{ij} \mathcal{H}_{ij} H_i \right] \right)^\top P \left( E - LD \right) \right] w_k \\
& + w_k^\top \left[ \left( E - LD \right)^\top P \left( A - LC - L \sum_{i,j=1}^{p,n_i} \left[ \tilde{\phi}_{ij} \mathcal{H}_{ij} H_i \right] \right) \right] e_k
\end{aligned} \tag{28}
$$

**Box I.**

$$
\mathbb{N}_i = \textit{block-diag} \left( \mathbb{S}_{i1}, \ldots, \mathbb{S}_{in_i} \right), \tag{27}
$$

*then, the observation error system in (15) is asymptotically stable and the $\mathcal{H}_\infty$ performance criterion (19) is guaranteed with $\nu = \lambda_{\max}(P)$. In addition, the observer gain L is computed as*

$$
L = P^{-1} \mathcal{X}^\top.
$$

**Proof.** The proof of this theorem is an extension of the continuous-time case in Zemouche et al. (2017). By calculating $\mathcal{W}_k$ along the trajectories of (15), we obtain (28) given in Box I.

Then, (28) can be written as follows

$$
\mathcal{W}_k = \begin{bmatrix} e_k \\ w_k \end{bmatrix}^\top \begin{bmatrix} \mathbb{A}^\top P \mathbb{A} - P + \mathbb{I} & \mathbb{A}^\top P \mathbb{E} \\ (\star) & \mathbb{E}^\top P \mathbb{E} - \mu \mathbb{I} \end{bmatrix} \begin{bmatrix} e_k \\ w_k \end{bmatrix} \tag{29}
$$

It follows that $\mathcal{W}_k \leqslant 0$ if the following inequality holds

$$
\begin{bmatrix} \mathbb{A}^\top P \mathbb{A} - P + \mathbb{I} & \mathbb{A}^\top P \mathbb{E} \\ (\star) & \mathbb{E}^\top P \mathbb{E} - \mu \mathbb{I} \end{bmatrix} < 0, \tag{30}
$$

which is equivalent to

$$
\begin{bmatrix} -P + \mathbb{I} & 0 \\ (\star) & -\mu \mathbb{I} \end{bmatrix} + \begin{bmatrix} \mathbb{A}^\top P \\ \mathbb{E}^\top P \end{bmatrix} P^{-1} \begin{bmatrix} P\mathbb{A} & P\mathbb{E} \end{bmatrix} < 0. \tag{31}
$$

Using Schur lemma we deduce that $\mathcal{W}_k < 0$ if the following matrix inequality holds

$$
\begin{bmatrix} -P + \mathbb{I} & 0 & \mathbb{A}^\top P \\ (\star) & -\mu \mathbb{I} & \mathbb{E}^\top P \\ (\star) & (\star) & -P \end{bmatrix} < 0, \tag{32}
$$

which is equivalent to

$$
\begin{bmatrix} \begin{bmatrix} -P + \mathbb{I} & 0 \\ 0 & -\mu \mathbb{I} \end{bmatrix} & \begin{bmatrix} \left( A - LC - L \sum_{i,j=1}^{p,n_i} \left[ \tilde{\phi}_{ij} \mathcal{H}_{ij} H_i \right] \right)^\top P \\ \left( E - LD \right)^\top P \end{bmatrix} \\ (\star) & -P \end{bmatrix} < 0. \tag{33}
$$

Inequality (33) can be rewritten as (34) given in Box II.

From Young's inequality we have

$$
\mathbb{Y}_i^\top \mathbb{X}_{ij} + \mathbb{X}_{ij}^\top \mathbb{Y}_i \leqslant \frac{1}{2} \left( \mathbb{X}_{ij} + \mathbb{S}_{ij} \mathbb{Y}_i \right)^\top \mathbb{S}_{ij}^{-1} \overbrace{\left( \mathbb{X}_{ij} + \mathbb{S}_{ij} \mathbb{Y}_i \right)}^{\Pi_{ij}}
$$

for any symmetric positive definite matrices $\mathbb{S}_{ij}$. Therefore, from (13) and the fact that $a_{ij} = 0$, inequality (34) holds if

$$
\mathbb{M} + \sum_{i,j=1}^{p,n_i} \left( \Pi_{ij}^\top \left( \frac{2}{\tilde{b}_{ij}} \mathbb{S}_{ij} \right)^{-1} \Pi_{ij} \right) < 0. \tag{35}
$$

Hence, by Schur lemma and the change of variable $\mathcal{X} = L^\top P$, inequality (35) is equivalent to (21). This ends the proof.

**Remark 2.** The convex optimization problem (20)–(21) in Theorem 1 does not depend explicitly on $\nu$ and then this value is not optimized. Indeed, we considered only the standard cost function used in $\mathcal{H}_\infty$ context. However, we can introduce $\nu$ in the convex optimization problem by adding constraint. Since $\nu = \lambda_{\max}(P)$, we can introduce a new scalar slack variable $\bar{\nu}$ and include the inequality $P < \bar{\nu} \mathbb{I}_n$. In this case, to optimize both $\mu$ and $\bar{\nu}$, we need to modify the cost function. Instead of (20), we have to use other cost functions depending on $\nu$, like

$$
\min \left( \max \left( \mu, \bar{\nu} \right) \right) \text{ subject to (21) and } P < \bar{\nu} \mathbb{I}_n
$$

or

$$
\min \left( \alpha \mu + \beta \bar{\nu} \right) \text{ subject to (21) and } P < \bar{\nu} \mathbb{I}_n
$$

where $\alpha$ and $\beta$ can be fixed by the user with respect to the objectives at hand.

### 3.3. On feasibility of (21) for non-monotonic outputs

The following theorem provides the non-existence of a constant observer gain solution for the non-monotonic LED-based optical communication model under the existence of a quadratic Lyapunov function.

**Theorem 2.** *Assume that the two following items hold:*

*(i) All the nonlinear output functions $h_i, i = 1, \ldots, p$, are non-monotonic;*
*(ii) the system matrix A is not Schur stable.*

*Then the LMI (21) is infeasible.*

**Proof.** First, consider the following change of variables

$$
\mathbb{T}_{ij} = \frac{2}{\tilde{b}_{ij}} \mathbb{S}_{ij} \quad \text{and} \quad \widetilde{\mathbb{N}} = \Lambda \mathbb{N}.
$$

Then, the LMI (21) in Theorem 1 is equivalent to

$$
\begin{bmatrix} \mathbb{M} & \begin{bmatrix} \nabla_1^\top & \cdots & \nabla_p^\top \end{bmatrix} \\ (\star) & -\widetilde{\mathbb{N}} \end{bmatrix} < 0, \tag{36}
$$

$$\overbrace{\begin{bmatrix}\begin{bmatrix}-P+\mathbb{I} & 0\\ 0 & -\mu\mathbb{I}\end{bmatrix} & \begin{bmatrix}A^\top P - C^\top L^\top P\\ E^\top P - D^\top L^\top P\end{bmatrix}\\ (\star) & -P\end{bmatrix}}^{\mathbb{M}} + \sum_{i,j=1}^{p,n_i}\tilde{\phi}_{ij}\left(\overbrace{\begin{bmatrix}H_i^\top\\0\\0\end{bmatrix}}^{\mathbb{Y}_i^\top}\overbrace{\begin{bmatrix}0 & 0 & -\mathcal{H}_{ij}^\top L^\top P\end{bmatrix}}^{\mathbb{X}_{ij}} + \mathbb{X}_{ij}^\top\mathbb{Y}_i\right) < 0. \tag{34}$$

**Box II.**

where

$$\mathbb{M} = \begin{bmatrix}-P+\mathbb{I}_n & 0 & A^\top P - C^\top\mathcal{X}\\ (\star) & -\mu\mathbb{I}_z & E^\top P - D^\top\mathcal{X}\\ (\star) & (\star) & -P\end{bmatrix}, \tag{37}$$

$$\nabla_i = \left[\nabla_{i1}^\top(\mathcal{X},\mathbb{T}_{i1})\dots\nabla_{in_i}^\top(\mathcal{X},\mathbb{T}_{in_i})\right]^\top,$$
$$\nabla_{ij}^\top(\mathcal{X},\mathbb{T}_{ij}) = \begin{bmatrix}0\\0\\-\mathcal{X}^\top\mathcal{H}_{ij}\end{bmatrix} + \frac{\tilde{b}_{ij}}{2}\begin{bmatrix}H_i^\top\\0\\0\end{bmatrix}\mathbb{T}_{ij}. \tag{38}$$

To simplify the proof, we will use a compact form of (36). To this end, we introduce the following notation

$$\mathcal{G} \triangleq \left[\mathcal{H}_{11}\dots\mathcal{H}_{in_1}\dots\mathcal{H}_{p1}\dots\mathcal{H}_{pn_p}\right],$$
$$\mathcal{H}^\top \triangleq \left[\underbrace{H_1^\top\dots H_1^\top}_{n_1\text{times}}\dots\underbrace{H_p^\top\dots H_p^\top}_{n_p\text{times}}\right].$$

We also define $\Gamma_a$ and $\Gamma_b$ in the same diagonal form as $\Lambda$ by replacing $\frac{2}{\tilde{b}_{ij}}$ with $a_{ij}$ and $b_{ij}$, respectively. Then, LMI (36) can be written under the compact form

$$\begin{bmatrix}\mathbb{M} & -\begin{bmatrix}0\\0\\P\mathcal{L}\mathcal{G}\end{bmatrix} + \begin{bmatrix}\mathcal{H}^\top\\0\\0\end{bmatrix}\left(\overbrace{\frac{\Gamma_b-\Gamma_a}{2}}^{\Lambda^{-1}}\right)^\top\widetilde{\mathbb{N}}\\ (\star) & -\widetilde{\mathbb{N}}\end{bmatrix} < 0. \tag{39}$$

Since from $(i)$ all the nonlinear functions $h_j$ are non-monotonic, then from the definition of $C$ in (14), we deduce that

$$C = \mathcal{G}\Gamma_a\mathcal{H}. \tag{40}$$

This compact form expression of the matrix $C$ is essential and plays an important role to proof infeasibility of the LMI for the LED model. It follows that $\mathbb{M}$ in (37) can be decomposed as

$$\mathbb{M} = \begin{bmatrix}-P+\mathbb{I}_n & 0 & A^\top P\\ (\star) & -\mu\mathbb{I}_z & E^\top P - D^\top\mathcal{X}\\ (\star) & (\star) & -P\end{bmatrix} - \begin{bmatrix}0\\0\\P\mathcal{L}\mathcal{G}\end{bmatrix}\Gamma_a\begin{bmatrix}\mathcal{H} & 0 & 0\end{bmatrix} - \begin{bmatrix}\mathcal{H}^\top\\0\\0\end{bmatrix}\Gamma_a^\top\begin{bmatrix}0\\0\\P\mathcal{L}\mathcal{G}\end{bmatrix}^\top \tag{41}$$

Hence from Schur lemma and the decomposition (41), LMI (39) is equivalent to (42). On the other hand, after some manipulations, the LMI (42) is identically written under the form (43), which brings out the monotonicity through the term $\Gamma_a^\top\widetilde{\mathbb{N}}\Gamma_b + \Gamma_b^\top\widetilde{\mathbb{N}}\Gamma_a$ (Eqs. (42) and (43) are given in Boxes III and IV). Hence, if all the nonlinearities are non-monotonic, *i.e.*

$$\Gamma_a^\top\widetilde{\mathbb{N}}\Gamma_b + \Gamma_b^\top\widetilde{\mathbb{N}}\Gamma_a < 0, \tag{44}$$

then the feasibility of (43) implies

$$\begin{bmatrix}-P+\mathbb{I}_n & 0 & A^\top P\\ (\star) & -\mu\mathbb{I}_z & E^\top P - D^\top\mathcal{X}\\ (\star) & (\star) & -P\end{bmatrix} < 0. \tag{45}$$

Let

$$\Omega = \begin{bmatrix}\mathbb{I}_n & 0 & 0\\ 0 & 0 & \mathbb{I}_n\\ 0 & \mathbb{I}_z & 0\end{bmatrix},$$

then inequality (45) is equivalent to

$$\Omega^\top\begin{bmatrix}-P+\mathbb{I}_n & 0 & A^\top P\\ (\star) & -\mu\mathbb{I}_z & E^\top P - D^\top\mathcal{X}\\ (\star) & (\star) & -P\end{bmatrix}\Omega < 0, \tag{46}$$

which is identical to

$$\begin{bmatrix}-P+\mathbb{I}_n & A^\top P & 0\\ (\star) & -P & PE - \mathcal{X}^\top D\\ (\star) & (\star) & -\mu\mathbb{I}_z\end{bmatrix} < 0. \tag{47}$$

It follows that from (47) we have necessarily

$$\begin{bmatrix}-P+\mathbb{I}_n & A^\top P\\ (\star) & -P\end{bmatrix} < 0 \tag{48}$$

which means that $A$ is Schur stable. This contradicts item $(ii)$ of Theorem 2. Then if the matrix $A$ is not Schur stable, the LMI (21) is infeasible. This ends the proof.

Three conclusions can be derived from Theorem 2.

- **(i)** The proposed LMI (21) remains still infeasible even if the observer gain $L$ is time-varying. Indeed, it is quite clear from the LMI (21) that the proof of infeasibility does not depend on the gain $L$, which is not inside the diagonal term in the LMI (21). On the other hand, if a time-varying gain is used to overcome infeasibility of the LMI (21), it will be mandatory to proceed with a different manner to get a new LMI condition, where infeasibility will depend on the observer parameters.
- **(ii)** It is worth mentioning that the goal is to facilitate the use of Young inequality and focus only on the matrices. With $a_{ij} < 0$, for example, we cannot apply the Young inequality to get the LMI condition of Theorem 1. The matrices $\Gamma_a$ and $\Gamma_b$ are introduced and used in the proof of Theorem 2 because all the properties of the nonlinearities should be accounted in the proof of infeasibility. Furthermore, the non-monotonicity is characterized by both $a_{ij}$ and $b_{ij}$, then by $\Gamma_a$ and $\Gamma_b$, with $\Gamma_a < 0$ and $\Gamma_b > 0$.
- **(iii)** Note that the non-monotonicity does not directly imply inequality (44) holds for any general symmetric and positive definite matrix $\widetilde{\mathbb{N}}$. However, due to the structure of $\widetilde{\mathbb{N}}$ and (more essential) the structure of $\Gamma_a$ and $\Gamma_b$ (each matrix block $\mathbb{S}_{ij}$ is multiplied by a scalar $a_{ij}$ and $b_{ij}$, respectively

$$\begin{bmatrix} -P+\mathbb{I} & 0 & A^\top P \\ (\star) & -\mu\mathbb{I} & E^\top P - D^\top \mathcal{X} \\ (\star) & (\star) & -P \end{bmatrix} - \begin{bmatrix} 0 \\ 0 \\ PL\mathcal{G} \end{bmatrix} \Gamma_a \begin{bmatrix} \mathcal{H} & 0 & 0 \end{bmatrix} - \begin{bmatrix} \mathcal{H}^\top \\ 0 \\ 0 \end{bmatrix} \Gamma_a^\top \begin{bmatrix} 0 & 0 & \left(PL\mathcal{G}\right)^\top \end{bmatrix}$$
$$+ \left( - \begin{bmatrix} 0 \\ 0 \\ PL\mathcal{G} \end{bmatrix} + \frac{1}{2} \begin{bmatrix} \mathcal{H}^\top \\ 0 \\ 0 \end{bmatrix} \left( \overbrace{\Gamma_b - \Gamma_a}^{\Lambda^{-1}} \right)^\top \widetilde{\mathbb{N}} \right) \widetilde{\mathbb{N}}^{-1} \left( - \begin{bmatrix} 0 \\ 0 \\ PL\mathcal{G} \end{bmatrix} + \frac{1}{2} \begin{bmatrix} \mathcal{H}^\top \\ 0 \\ 0 \end{bmatrix} \left( \overbrace{\Gamma_b - \Gamma_a}^{\Lambda^{-1}} \right)^\top \widetilde{\mathbb{N}} \right)^\top < 0. \tag{42}$$

**Box III.**

$$\begin{bmatrix} -P+\mathbb{I} & 0 & A^\top P \\ (\star) & -\mu\mathbb{I} & E^\top P - D^\top \mathcal{X} \\ (\star) & (\star) & -P \end{bmatrix} - \frac{1}{2} \begin{bmatrix} \mathcal{H}^\top \\ 0 \\ 0 \end{bmatrix} \overbrace{\left[ \Gamma_a^\top \widetilde{\mathbb{N}} \Gamma_b + \Gamma_b^\top \widetilde{\mathbb{N}} \Gamma_a \right]}^{<0} \begin{bmatrix} \mathcal{H} & 0 & 0 \end{bmatrix}$$
$$+ \underbrace{\left( - \begin{bmatrix} 0 \\ 0 \\ PL\mathcal{G} \end{bmatrix} + \frac{1}{2} \begin{bmatrix} \mathcal{H}^\top \\ 0 \\ 0 \end{bmatrix} \left( \Gamma_b + \Gamma_a \right)^\top \widetilde{\mathbb{N}} \right) \widetilde{\mathbb{N}}^{-1} \left( - \begin{bmatrix} 0 \\ 0 \\ PL\mathcal{G} \end{bmatrix} + \frac{1}{2} \begin{bmatrix} \mathcal{H}^\top \\ 0 \\ 0 \end{bmatrix} \left( \Gamma_b + \Gamma_a \right)^\top \widetilde{\mathbb{N}} \right)^\top}_{>0} < 0. \tag{43}$$

**Box IV.**

for a couple $(i, j)$), then non-monotonicity implies (44). Hence, this justifies and confirms the matrix $\widetilde{\mathbb{N}}$ to be block-diagonal form from the application of Young's inequality, rather than be a general symmetric and positive definite matrix.

### 3.4. A switched-gain based observer as a solution

It has recently been proven in the continuous-time case (Rajamani et al., 2020) that when all the nonlinear output functions are non-monotonic, a single observer gain that guarantees exponentially stable estimation error over the entire operating range cannot be found. Consequently, the LMI (21) is not feasible. Contrary to what has been indicated in Rajamani et al. (2020), the LMI (21) is not feasible since the observer gain is constant. However, it remains infeasible even for time-varying gain in case of non-monotonicity of all the output functions $h_i(.)$. It is due to the design procedure and the exploitation of the nonlinearities related assumptions. Different observer design methods that use a time-varying gain jointly with a new way to handle the nonlinearities and introduce output transformations exist. However, if we want to keep LMI (21) and exploit it for the observer design, then the unique solution is to introduce a switched-gain based observer as depicted in Figs. 4 and 5.

The goal consists of designing a switched-gain observer that uses observer gains and a hysteresis to make the observer error dynamics globally asymptotically stable. Indeed, the basic idea of this switched-gain strategy consists of combining, for example, two constant-gain regions, as shown in Fig. 4, with no loss of generality. The switched-gain is designed so that around the nominal switch point $y^* = y_{\text{switch}}$ between, for example, two regions and the hysteresis variable $\varepsilon$, the observer error dynamic guarantees convergence. To proceed, we consider a switched-gain observer with a constant-gain $L_i$ in the region $R_i$ designed using the LMI (21) with $\Gamma_{a_{R_i}}$, $\Gamma_{b_{R_i}}$, and the corresponding value of the quadratic Lyapunov positive definite matrix $P_i$ as shown in Fig. 4 in the case of switching between two regions. In Fig. 4, the parameter $\varepsilon$ is the hysteresis added to the switching to ensure a minimum dwell time after each switch (Rajamani et al., 2020). The stability of the switched-gain observer of Fig. 4 consisting of different constant observer gain regions needs to be considered. Note that the proposed switching-gain strategy selects the current mode of operation of a switched system based on the nominal value of the output $y^* = y_{\text{switch}}$ for each region, as illustrated in Fig. 5. Subsequently, the switching strategy utilizes the notion of dwell time, which has been widely used in control techniques, see for instance (Branicky, 1998; Mayhew et al., 2011; Peleties & DeCarlo, 1991; Sanfelice, 2021). The number of regions involved depends on how non-monotonic the involved functions are and how many zero-slope points are involved in these nonlinear functions. As more zero-slope points occur in the non-monotonic function, more switching regions are needed.

Let the observers be designed to be asymptotically stable in each of the switching regions using the quadratic Lyapunov function analysis of Theorem 1. Then, it should be noted that inside each region, a single observer gain is used, and asymptotic stability is guaranteed under the constraint of feasibility of (21). Furthermore, the stability of the overall switched system can be guaranteed if the system satisfies a minimum dwell time constraint in each region and the results from switching system theory (Alessandri et al., 2005; Goebel et al., 2012; Liberzon, 2003).

**Remark 3.** Let $y_{\text{switch}}$ and $L_i$ be the nominal switching point between the two regions and observer gains respectively so that asymptotically stable switched-observers gains are designed and for some positive parameter $\varepsilon$, the value of the output function is such that there exists $i^+$ for which

$$y^i \geqslant y_{\text{switch}}^{i+} + \varepsilon, \tag{49}$$

then the switched-gain observer strategy updates $i$ to $i^+$ ($i^+$ denotes the value of $i$ after the switch) and applies to the observer dynamics the observer gain matrix associated to the new value of $i$. Note that condition (49) determines the situation when switching to the observer gain associated with $i^+$ occurs when the observer error is far to the slope points.

The proposed switched-gain based observer can be summarized as follows

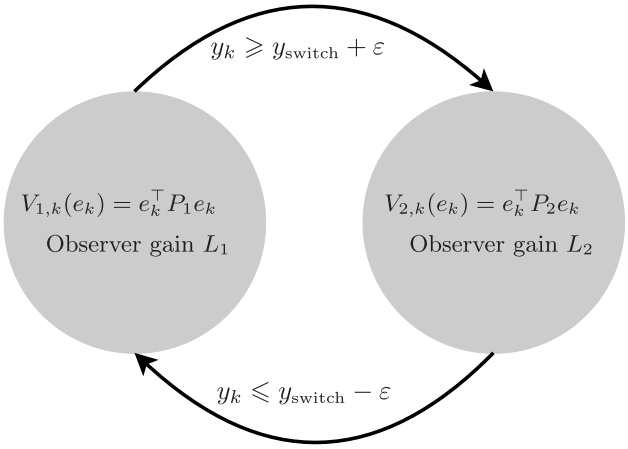


**Fig. 4.** Discrete-time observer with switched gains.

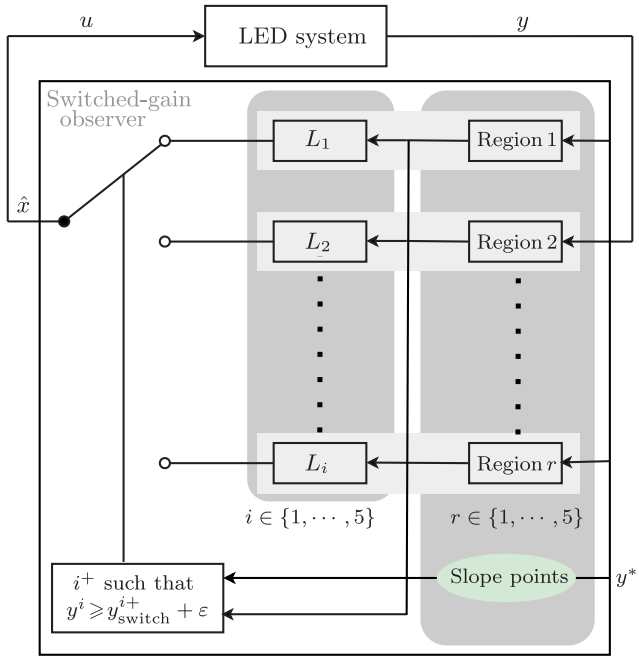


**Fig. 5.** Switched-gain based observer design where $i^+ \in \{r \in \{1, \ldots, 5\} : \ y^i \geqslant y^{i+}_{\text{switch}} + \varepsilon\}$.

- When the observer gain $L_i$ is applied to the LED system for given $\varepsilon$, apply it as long as

$$y^i \leqslant y^{i+}_{\text{switch}} - \varepsilon, \qquad \forall r \in \{1, \ldots, 5\}, \tag{50}$$

  then $i$ is constant when (50) holds (i.e. when $y$ is close to $y_{\text{switch}}$).
- When

$$y^i \geqslant y^{i+}_{\text{switch}} + \varepsilon, \tag{51}$$

  for $r \in \{1, \ldots, 5\}$, then update $i$ according to (i.e. when $y$ is far from $y_{\text{switch}}$).

$$i^+ \in \{r \in \{1, \ldots, 5\} : \ y^i \geqslant y^{i+}_{\text{switch}} + \varepsilon\}, \quad \forall i^+ = r.$$

The largest decay rate $\sigma$ of system (10) is defined such that

$$\lim_{k \longrightarrow \infty} \exp(\sigma k) \|e_k\| = 0, \tag{52}$$

holds for $w_k \equiv 0$ and for all trajectories $e_k$. We can use the quadratic Lyapunov function $V(e_k) = e_k^\top P e_k$ to obtain a lower bound of the error dynamics (15). From (21), it implies that

$$\Delta V(e_k) \leqslant -\sigma e_k^\top e_k. \tag{53}$$

From (53) and the fact that

$$\lambda_{\min}(P) \|e_k\|^2 \leqslant V(e_k) \leqslant \lambda_{\max}(P) \|e_k\|^2, \tag{54}$$

we have

$$\|e_k\| \leqslant \sqrt{\frac{\lambda_{\max}(P)}{\lambda_{\min}(P)}} \|e(0)\| \exp\left(-\frac{k\sigma}{\lambda_{\max}(P)}\right). \tag{55}$$

Hence, the inequality (55) means that the observer error converges exponentially to zero with the minimum decay rate $\sigma$.

For a finite set of piecewise regions with the monotonicity that is guaranteed in each region, we can state the condition that ensures a globally asymptotically stable switched-gain observer with guaranteed disturbance level and decay rate. For the sake of simplicity, the following proposition considers only two regions.

**Proposition 3.** *Let $P_1$, $L_1$, $\mu_1$ and $P_2$, $L_2$, $\mu_2$ be the Lyapunov function matrices, observer gain matrices and disturbance attenuation levels in regions 1 and 2 respectively, chosen so as to satisfy (21). Let $\sigma_1, \sigma_2 \in (0, 1)$ be the minimum convergence rates in the two regions. Choose a value of $r$ such that the following equations are guaranteed*

$$P_1 \geqslant \sigma_2^{r-1} P_2, \tag{56}$$

*and*

$$P_2 \geqslant \sigma_1^{r-1} P_1, \tag{57}$$

*then, if the switching between regions does not occur faster than $r \in \mathbb{N}_+$ times of sampling period, the switched-gain observer system will be globally asymptotically stable with guaranteed attenuation gain $\mu = \max\{\mu_i\}_{i \in \{1,2\}}$.*

**Proof.** To ensure the decay rate $\sigma > 0$, we need $\Delta V_i(e_k) < -2\sigma V_i(e_k)$ instead of $\Delta V_i(e_k) < 0$, hence this adds the term $\{2\sigma_i P_i\}_{i \in \{1,2\}}$ in the first row-column of $\mathbb{M}$ in (22). Now, consider the case where the observer gain switches from $L_1$ to $L_2$ for $w_k \equiv 0$. Since $\sigma_2$ is assumed to be the minimum convergence rate of region 2, we have $V_2(k+1) \leqslant \sigma_2 V_2(k)$ and $\Delta V_2(e_k) + \sigma_2 V_2(e_k) = e_k^\top \widetilde{\Sigma} e_k$ where

$$\widetilde{\Sigma} = \begin{bmatrix} \widetilde{\mathbb{M}} & \begin{bmatrix} \Pi_1^\top & \cdots & \Pi_p^\top \end{bmatrix} \\ (\star) & -\Lambda \mathbb{N} \end{bmatrix} < 0, \tag{58}$$

and

$$\widetilde{\mathbb{M}} = \begin{bmatrix} -P_2 + \mathbb{I}_n & A^\top P_2 - C^\top \mathcal{X} \\ (\star) & -(1 - \sigma_2) P_2 \end{bmatrix},$$

$C$ is designed in the operating regions of interest due to the monotonicity concept. From the LMI (21), we know that $\Sigma < 0$ which implies by Schur complement that $\widetilde{\Sigma} < 0$ for $w_k \equiv 0$. On the other hand, suppose at $k_s \in \mathbb{N}_+$, the observer intends to switch between the two regions. By assumption, the exact switching can only happen at or after $k_s + r$, and we have

$$V_2(k_s + r) \leqslant \sigma_2^r V_2(k_s).$$

Equivalently, that is

$$e_{k_s+r}^\top P_2 e_{k_s+r} \leqslant \sigma_2^r e_{k_s}^\top P_2 e_{k_s}.$$

By (56), it follows that

$$V_2(k_s + r) = e_{k_s+r}^\top P_2 e_{k_s+r} \leqslant \sigma_2 e_{k_s}^\top P_1 e_{k_s} = \sigma_2 V_1(k_s).$$

After entering region 2 at $k_s + r$, $V_2(k)$ will keep decreasing monotonically in region 2. Similarly, we can show that $V_1(k_s+r) \leqslant \sigma_1 V_2(k_s)$ for a switching from region 2 to 1 intended at any $k_s \in \mathbb{N}_+$ for $w_k \equiv 0$. If the observer stays in one region after a finite time of switching, $e_k$ will converge to zero since the observer error dynamics is globally asymptotically stable for $w_k \equiv 0$. Now, consider $w_k \neq 0$, one has $\Delta V_2(e_k) + \sigma_2 V_2(e_k) + e_k^\top e_k - \mu_i^2 w_k^\top w_k = \xi_k^\top \bar{\Sigma} \xi_k$ where $\xi_k = [e_k^\top \; w_k^\top]^\top$ and

$$\bar{\Sigma} = \begin{bmatrix} \mathbb{A}^\top P \mathbb{A} - P + \mathbb{I} & \mathbb{A}^\top P \mathbb{E} \\ (\star) & \mathbb{E}^\top P \mathbb{E} - \mu_2 \mathbb{I} \end{bmatrix}.$$

From the LMI (21), $\Sigma < 0$ is equivalent to $\bar{\Sigma} < 0$ for all $w_k \neq 0$. Therefore, one has $\Delta V_2(e_k) \leqslant -\sigma_2 V_2(e_k) + e_k^\top e_k - \mu_i^2 w_k^\top w_k$ for all $w_k \neq 0$ by which ends the proof.

**Remark 4.** To support the general case where the switching rule moves back and forth, one can assume the switching starts from region 1 without loss of generality, and let $\{k_1^\kappa, k_1^{\bar{\kappa}}, \ldots, k_m^{\bar{\kappa}}, \ldots\}$ be the sequence of time indices when the observer intends to switch from one region to another. The superscript "$\kappa$" ("$\bar{\kappa}$") represents a switching from region 1 (2) to region 2 (1). By our assumption,

$$k_m^\kappa + r \leqslant k_m^{\bar{\kappa}}, \quad k_m^{\bar{\kappa}} + r \leqslant k_{m+1}^\kappa$$

for all positive integer $m$. Therefore, we have

$$V_2(k_m^{\bar{\kappa}}) \leqslant V_2(k_m^\kappa + r) \leqslant \sigma_2 V_1(k_m^\kappa),$$
$$V_1(k_{m+1}^\kappa) \leqslant V_1(k_m^{\bar{\kappa}} + r) \leqslant \sigma_1 V_2(k_m^{\bar{\kappa}}),$$

for all positive integer $m$. It follows that

$$V_1(k_m^\kappa) \leqslant (\sigma_1\sigma_2)^{m-1} V_1(k_1^\kappa),$$
$$V_2(k_{m+1}^{\bar{\kappa}}) \leqslant \sigma_1^m \sigma_2^{m+1} V_1(k_1^\kappa)$$

for all positive integer $m$. Since $\sigma_1, \sigma_2 \in (0, 1)$, both $V_1(k_m^\kappa)$ and $V_2(k_m^{\bar{\kappa}})$ converge to zero as $m \to \infty$. Hence, by following the same steps in the proof of Proposition 3, one can state that the switched-gain observer system is globally asymptotically stable with guaranteed decay rate and disturbance level $\mu = \max\{\mu_i\}_{i\in\{1,2\}}$ in each region. This completes the proof.

### 3.5. Numerical design procedure

The switching-gain based observer procedure is summarized in Algorithm 1, which will be implemented in Section 4 to illustrate the performances of the proposed methodology in Theorem 1. The two following points are essential before proceeding to the algorithm.

- In our LED setup, there are two sensors (output functions) and five switching regions in total, which are the minimal setup to achieve both observability and output monotonicity[2] such that the infeasibility issue of Theorem 2 is avoided.
- Note that each output function can be written as $h_i(x_1, x_2)$. From the system model, we notice that $h_i$ is monotonic w.r.t. $x_1$ while non-monotonic w.r.t. $x_2$. Therefore, the $x_1 - x_2$ plane is cut into five stripes w.r.t. $x_2$ such that in each of these stripes, either $h_1$ and/or $h_2$ is monotonic w.r.t. $x_2$. We denote the range of $x_1$ by $[\Phi_1, \Phi_2]$ and the range of $x_2$ is cut into $[l_1, r_1] \cup \cdots \cup [l_5, r_5]$. Hence the $i$th switching region is defined as $[\Phi_1, \Phi_2] \times [l_i, r_i]$.

[2] Minimal in terms of the number of sensors and switching regions such that there is at least one monotonic output function in each region.

**Algorithm 1.** Computation of the region gain.
**Result:** Observer gains $L_1, \ldots, L_r$ for each region
**Data:** Boundary of regions $[\Phi_1, \Phi_2] \times [l_k, u_k]$ for $k = 1, \ldots, r$; Coefficients of output functions $h_1, h_2$
**for** $k \leftarrow 1$ **to** $r$ **do**
  **Initialization**: $C^{(k)} \leftarrow \begin{bmatrix} 0 & 0 & 0 \\ 0 & 0 & 0 \end{bmatrix}$; flag $\leftarrow$ FALSE;
  **for** $i \leftarrow 1$ **to** 2 **do**
    /* $h_i$ is monotonic w.r.t. $x_1$ */
    $a_{i1}^{(k)} \leftarrow \min_{(t_1,t_2)\in[\Phi_1,\Phi_2]\times[l_k,u_k]} \frac{\partial h_i}{\partial x_1}(t_1, t_2)$;
    $b_{i1}^{(k)} \leftarrow \max_{(t_1,t_2)\in[\Phi_1,\Phi_2]\times[l_k,u_k]} \frac{\partial h_i}{\partial x_1}(t_1, t_2)$;
    /* $h_i$ might be non-monotonic w.r.t. $x_2$ in some regions */
    $a_{i2}^{(k)} \leftarrow \min_{(t_1,t_2)\in[\Phi_1,\Phi_2]\times[l_k,u_k]} \frac{\partial h_i}{\partial x_2}(t_1, t_2)$;
    $b_{i2}^{(k)} \leftarrow \max_{(t_1,t_2)\in[\Phi_1,\Phi_2]\times[l_k,u_k]} \frac{\partial h_i}{\partial x_2}(t_1, t_2)$;
    **if** $a_{i2}^{(k)} b_{i2}^{(k)} < 0$ and *flag == FALSE* **then**
      **if** *i==2* **then**
        TERMINATE since the LMI (21) is infeasible by Theorem 2;
      **else**
        Do nothing;
      **end**
    **else**
      flag $\leftarrow$ TRUE;
    **end**
    $H_i \leftarrow \begin{bmatrix} 1 & 0 & 0 \\ 0 & 1 & 0 \end{bmatrix}$;
    $C^{(k)} \leftarrow C^{(k)} + a_{i1}^{(k)} \mathcal{H}_{i1} H_i + a_{i2}^{(k)} \mathcal{H}_{i2} H_i$;
    $\tilde{b}_{i1} \leftarrow b_{i1}^{(k)} - a_{i1}^{(k)}$;
    $\tilde{b}_{i2} \leftarrow b_{i2}^{(k)} - a_{i2}^{(k)}$;
  **end**
  use the data computed for both sensors to construct LMI (21);
  $L_k \leftarrow$ solve LMI constrained optimization problem (20)–(21);
**end**

## 4. Application to the LED model

This section illustrates the theoretical contributions presented in the previous sections. The effectiveness of the proposed discrete-time nonlinear switched-gain observer is evaluated for the LED-based optical communication system. To do so, we consider the problem of estimating $x_{1,k}$, $\phi \triangleq x_{2,k}$ and $\dot{\phi} \triangleq x_{3,k}$ based on which the control $u_k$ is designed to drive the states $x_{2,k}$ and $x_{3,k}$ towards zero, which is the orientation with the maximum light intensity. The process dynamics of the LED model (7) are linear while the output equations (9) are nonlinear. It is also clear that $g(.)$ is function of the state $x_{2,k}$. Using the discrete-time nonlinear switched-gain observer (11), the nonlinear output functions $y_k$ are monotonic in the operating ranges of $x_{1,k}$ and $\phi \triangleq x_{2,k}$ as illustrated in Fig. 6. Hence, a constant observer gain matrix $L_i$ exists in the operating ranges of interest. However, it is impossible to find a constant gain matrix of $L_i$ with the exploitation of the LMI-based approach and the quadratic Lyapunov function that makes the observer stable for the entire operating range. Therefore, a switched gain based observer is needed for the allowable operating regimes. The next subsection describes the regions of monotonicity and how the observer switches between different modes.

The nonlinear output functions are divided piece-wise into different regions. In each region, at least one of the output functions is a monotonic function. Fig. 6 illustrates a piece-wise division of

**Table 2**
Operating ranges of $\phi$ [rad] and corresponding switched-gain observer gains.

| Region | Left [rad] | Right [rad] | Observer gain ($L$) | Optimal attenuation level $\sqrt{\mu}$ |
|---|---|---|---|---|
| 1 | −0.1745 | −0.0637 | $\begin{bmatrix} 0.8662 & -0.8619 \\ -1.1690 & 2.6077 \\ -11.6979 & 26.1265 \end{bmatrix}$ | 100.4965 |
| 2 | −0.0637 | −0.0288 | $\begin{bmatrix} -0.6757 & -0.1868 \\ -1.6321 & 2.9010 \\ -29.0384 & 51.6229 \end{bmatrix}$ | 100.1578 |
| 3 | −0.0288 | 0.1457 | $\begin{bmatrix} 0.4711 & 0.7361 \\ -1.7227 & 1.5778 \\ -13.1396 & 12.0346 \end{bmatrix}$ | 100.8566 |
| 4 | 0.1457 | 0.1806 | $\begin{bmatrix} -0.1367 & 0.6327 \\ -2.1472 & 0.8637 \\ -57.4492 & 23.1061 \end{bmatrix}$ | 100.0698 |
| 5 | 0.1806 | 0.2618 | $\begin{bmatrix} -1.1083 & 0.6851 \\ -2.7108 & 0.7248 \\ -28.2802 & 7.5478 \end{bmatrix}$ | 100.4578 |

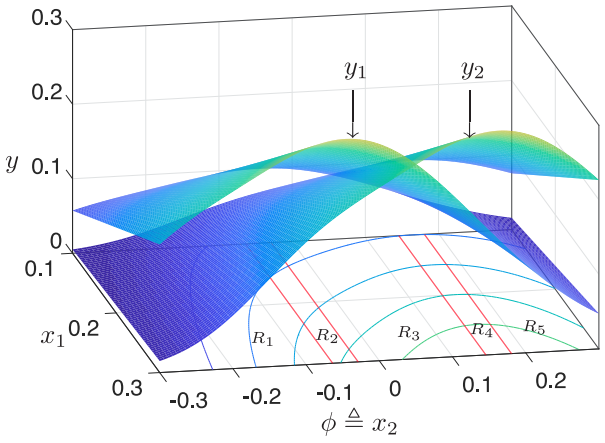


**Fig. 6.** Regions around slope-change points of the nonlinear output functions $y_k$.

the nonlinear output functions in the operating regions of interest due to the monotonicity concept. We note that the regions' boundaries lie at the slope change points. For example, $R_2$ is a narrow region where the nonlinear output function's slope $y_1$ is close to zero. In this region, only the output $y_2$ will be used by the observer since $y_2$ is monotonic. Regions $R_1$ and $R_3$ lie on either side of $R_2$ and both of these regions can utilize both outputs $y_1$ and $y_2$. Both $y_1$ and $y_2$ are monotonic in these regions. Since each region of interest $R_1$ through $R_5$ has monotonic output function properties, as illustrated in Fig. 6. Then, a constant stabilizing observer gain exists in each of these regions. Table 2 provides the five operating regimes and their corresponding observer gains and optimal attenuation levels.

We analyze the capability of the proposed discrete-time nonlinear switched-gain observer synthesis method to reconstruct the states in comparison to a standard EKF (Anderson & Moore, 1979) based on the LED optical communication model (7)–(9). We assume that the process noise vector $w_k \sim \mathcal{N}(0, Q)$, and measurement noise $v_k \sim \mathcal{N}(0, R)$. The gain matrices for EKF are chosen using different settings of $Q$ and $R$, including the same covariance of the process and measurement noises. Figs. 7, 8, 9, 10 and 11 illustrate the estimation performance of the discrete-time switched-gain observer and the EKF for different choices of $Q$ and $R$. The proposed switched discrete-time nonlinear observer exhibits good estimation performance while the EKF fails to maintain a good estimation performance. Subsequently, the proposed discrete-time nonlinear switched-gain observer rejects the process and measurement noises. Table 3 summarizes the RMSE of the states and outputs errors for both nonlinear observer design and EKF over the interval time [0–5 s]. Roughly, the nonlinear observer outperforms the four EKF using different settings of $Q$ and $R$. Subsequently, the proposed nonlinear observer generates a better convergence error than the EKF.

**Remark 5.** Note that the higher values of the optimal attenuation level mean that the signal noise deviation (process and measurements) might be small. Even though the signal noise deviation is small, the disturbance rejection property is essential in the switched-gain framework since very small standard deviations can significantly affect the solutions to a switched-gain system. In particular, the switched times of the nominal solution between each switching region are likely different from those solutions in the presence of noise, no matter how small the noise perturbation function might be. Such mismatch can lead to large errors between the nominal and the disturbed system at a common time. Furthermore, as shown in the paper, even if the values of the optimal attenuation level are relatively high, it does not mean that the method is not beneficial as the proposed switched-gain-based technique works better than the EKF.

**Remark 6.** The optimal value of $\mu$ returned by the LMI synthesis conditions guarantees the $\mathcal{H}_\infty$ criterion for any $w_k \in \ell_2$, then it corresponds to the worst case. That is, for any $w_k \in \ell_2$, the designed observer remains $\mathcal{H}_\infty$ stable, and it will not exceed the returned value of $\mu$. In addition, the optimal value of $\mu$ depends on the matrices $E$ and $D$, which represent the distribution of the process dynamics and output measurements disturbances. Moreover, the resulting closed-loop disturbance gain once the observer is designed is $\sqrt{\mu} = 26.4249$.

## 5. Conclusion

We have designed a switched-gain observer framework in which the output nonlinearities are non-monotonic and depend on multi-dimensional variables. The designed observer is applied to an LED-based optical communication system. Based on this framework, sufficient conditions for the asymptotic stability and the $\mathcal{H}_\infty$ performance criterion of the observation error dynamics are guaranteed using Lyapunov-analysis. To the best of our knowledge, no constant observer gain results in the literature lead to feasible LMI for non-monotonic output measurement equations with multi-dimensional variables. The stability condition of the proposed switched-gain observer approach is based on the dwell-time method and quadratic Lyapunov functions. For

**Table 3**
RMSE states and output errors performance comparison: nonlinear observer versus EKF over the interval time [0–5 s].

| Design scheme | RMSE$_{x_1}$ [W] | RMSE$_{x_2}$ [Rad] | RMSE$_{x_3}$ [Rad/s] | RMSE$_{y_1}$ [W] | RMSE$_{y_2}$ [W] |
|---|---|---|---|---|---|
| Nonlinear observer | 0.0017 | **0.0047** | **0.1292** | **0.0023** | **0.0024** |
| EKF ($Q_1, R_1$) | 0.0010 | 0.0201 | 0.1368 | 0.0058 | 0.0076 |
| EKF ($Q_2, R_2$) | 0.0050 | 0.2843 | 0.1516 | 0.0458 | 0.0243 |
| EKF ($Q_3, R_3$) | 0.0010 | 0.0202 | 0.1360 | 0.0061 | 0.0074 |
| EKF ($Q_4, R_4$) | 0.0063 | 0.1228 | 0.1498 | 0.0447 | 0.0323 |

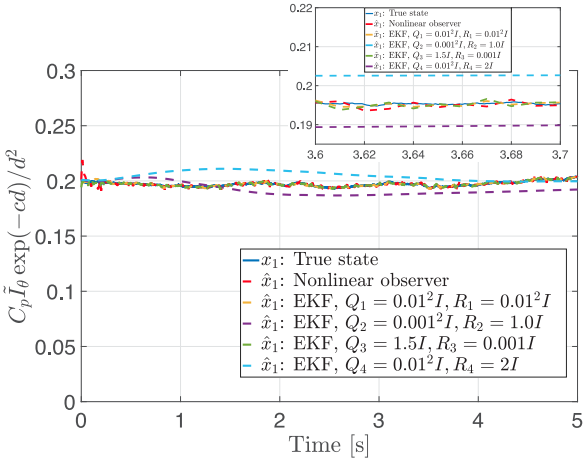


**Fig. 7.** Estimated state $\hat{x}_1$ along with the actual state $x_1$.

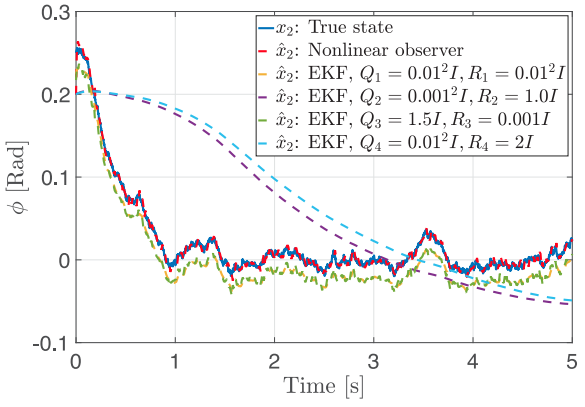


**Fig. 8.** Estimated state $\hat{x}_2$ along with the state $x_2$.

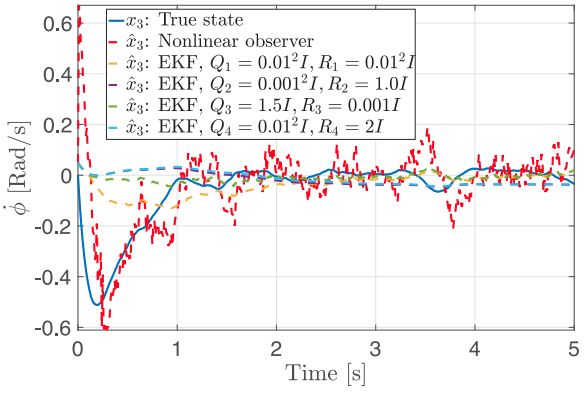


**Fig. 9.** Estimated state $\hat{x}_3$ along with the state $x_3$.

future work, one could benefit from non-monotonic Lyapunov functions that allow the dynamics of the switched system to be

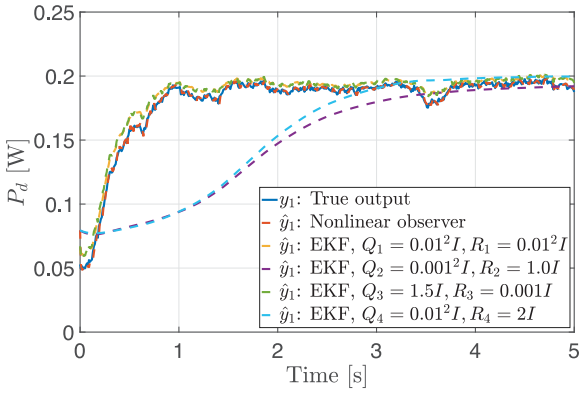


**Fig. 10.** Estimated output power $\hat{y}_1$ along with the actual output power $y_1$.

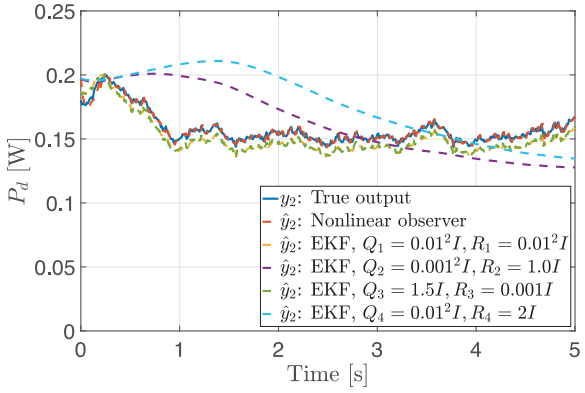


**Fig. 11.** Estimated output power $\hat{y}_2$ along with the actual output power $y_2$.

inferred in the Lyapunov function and overcome the infeasibility of the LMI conditions.

## References


Acikmese, B., & Corless, M. (2011). Observers for systems with nonlinearities satisfying incremental quadratic constraints. *Automatica*, *47*(7), 1339–1348.

Alessandri, A. (2003). Sliding-mode estimators for a class of non-linear systems affected by bounded disturbances. *International Journal of Control*, *76*(3), 226–236.

Alessandri, A., Baglietto, M., & Battistelli, G. (2005). Receding-horizon estimation for switching discrete-time linear systems. *IEEE Transactions on Automatic Control*, *50*(11), 1736–1748.

Alessandri, A., Donnarumma, S., Martelli, M., & Vignolo, S. (2019). Motion control for autonomous navigation in blue and narrow waters using switched controllers. *Journal of Marine Science and Engineering*, *7*(196), 1–15.

Alessandri, A., & Gaggero, M. (2019). Fast moving horizon state estimation for discrete-time systems with linear constraints. *Adaptive Control and Signal Processing*, *34*(6), 706–720.

Anderson, B., & Moore, J. (1979). *Optimal filtering*. Philadelphia, Englewood Cliffs, NJ: Prentice-Hall.

Arcak, M., & Kokotovic, P. (2001). Observer-based control of systems with slope-restricted nonlinearities. *IEEE Transactions on Automatic Control*, *46*(7), 1146–1150.

Borah, D., Boucouvalas, A., Davis, C., Hranilovic, S., & Yiannopoulos, K. (2012). A review of communication-oriented optical wireless systems. *EURASIP Journal on Wireless Communications and Networking*, *91*(3), 226–236.

Branicky, M. S. (1998). Multiple Lyapunov functions and other analysis tools for switched and hybrid systems. *IEEE Transactions on Automatic Control*, *43*(4), 475–482.
De-Vaul, R. W., Teller, E., Biffle, C. L., & Weaver, J. (2014). Balloon power sources with a buoyancy trade-off. United States Patent US2014/0 048 646A1.
Doniec, N., Angermann, M., & Rus, D. (2013). An end-to-end signal strength model for underwater optical communications. *IEEE Journal of Oceanic Engineering*, *38*(4), 743–757.
Draa, K. C., Zemouche, A., Alma, M., Voos, H., & Darouach, M. (2019). A discrete-time nonlinear state observer for the anaerobic digestion process. *International Journal of Robust and Nonlinear Control*, *29*(5), 1279–1301.
Elgala, H., Mesleh, R., & Haas, H. (2011). Indoor optical wireless communication: potential and state of-the-art. *IEEE Communications Magazine*, *49*(9), 56–62.
Elgala, H., Mesleh, R., & Haas, H. (2017). Optical communication in space: Challenges and mitigation techniques. *IEEE Communications on Survey Tutorials*, *19*(1), 57–96.
Ghassemlooy, Z., Popoola, W., & Rajbhandari, S. (2012). *Optical wireless communications: system and channel modelling with MATLAB* (1st ed.). Berlin: CRC Press.
Goebel, R., Sanfelice, R. G., & Teel, R. A. (2012). *Hybrid dynamical systems - modeling, stability, and robustness*. New Jersey: Princeton University Press.
Ha, Q., & Trinh, H. (2004). State and input simultaneous estimation for a class of nonlinear systems. *Automatica*, *40*, 1779–1785.
Hagem, R., Thiel, D. V., O'Keefe, S., Wixted, A., & Fickenscher, T. (2011). Low cost short-range wireless optical FSK modem for swimmers feedback. In *IEEE sensors conf.*. Los Angeles, CA, USA.
Hanson, F., & Radic, S. (2008). High bandwidth underwater optical communication. *Applied Optics*, *47*(2), 277–283.
Ivan, M., & Ching-Cherng, S. (2008). Modeling the radiation pattern of LEDs. *Optics Express*, *16*(3), 1808.
Lacerda, M. J., Tarbouriech, S., Garcia, G., & Peres, P. L. (2014). $\mathcal{H}_\infty$ Filter design for nonlinear polynomial systems. *Systems & Control Letters*, *70*, 77–84.
Li, H., & Fu, M. (1997). A linear matrix inequality approach to robust $\mathcal{H}_\infty$ filtering. *IEEE Transactions on Signal Processing*, *45*, 2338–2350.
Li, P., Lam, J., & Chesi, G. (2012). On the synthesis of linear $\mathcal{H}_\infty$ filters for polynomial systems. *Systems & Control Letters*, *61*, 31–36.
Liberzon, D. (2003). *Switching in systems and control*. New York: Springer.
Lu, F., Lee, S., Mounzer, J., & Schurgers, C. (2009). Low-cost medium-range optical under water modem. In *4th ACMint.workshop under water network* (pp. 1–11). Los Angeles, CA, USA.
Majumdar, A., & Ricklin, J. (2010). *Free-space laser communications: principles and advances*. Berlin: Springer.
Mayhew, C. G., Sanfelice, R. G., & Teel, A. R.
Miller, F., Vandome, A., & McBrewster, J. (2009). *Beer-lambert law*. Saarbrucken, Germany: VDM Publishing.
N'Doye, I., Zhang, D., Alouini, M.-S., & Laleg-Kirati, T.-M. (2018). Establishing and maintaining a reliable optical wireless communication in underwater environment. *IEEE Access*, *9*(2), 62519–62531.
N'Doye, I., Zhang, D., Zemouche, A., Rajamani, R., & Laleg-Kirati, T.-M. (2020). A switched-gain nonlinear observer for LED optical communication. In *21st ifac world congress*. Berlin, Germany.
Nov, A. (2018). Harnessing light for wireless communications. Available in https://code.fb.com/connectivity/harnessing-light-for-wireless-communications/.
Peleties, P., & DeCarlo, R. A. (1991). Asymptotic stability of *m*-switched systems using Lyapunov-like functions. In *Proceedings of the American Control Conference* (pp. 1679–1684).
Rajamani, R., Jeon, W., Movahedi, H., & Zemouche, A. (2020). On the need for switched-gain observers for non-monotonic nonlinear systems. *Automatica*, *114*, Article 108814.
Rajamani, R., Wang, Y., Nelson, G. D., Madson, R., & Zemouche, A. (2017). Observers with dual spatially separated sensors for enhanced estimation: Industrial, automotive, and biomedical applications. *IEEE Control Systems*, *37*(3), 42–58.
Rolf, F., Allgower, F., & Lorenz, B. (2007). *Assessment and Future Directions of Nonlinear Model Predictive Control*. New York: Springer.
Sanfelice, R. G. (2021). *Hybrid Feedback Control*. Princeton University Press.
Solanki, P. B., Al-Rubaiai, M., & Tan, X. (2016). Extended Kalman filter-aided alignment control for maintaining line of sight in optical communication. In *Proc. Amer. Control Conf.* (pp. 4520–4525).
Solanki, P. B., Al-Rubaiai, M., & Tan, X. (2018). Extended Kalman filter-based active alignment control for LED optical communication. *IEEE/ASME Transactions on Mechatronics*, *23*(4), 1501–1511.
Sontag, E. (1989). Smooth stabilization implies coprime factorization. *IEEE Transactions on Automatic Control*, *34*, 435–443.
Sontag, E., & Wang, Y. (1996). New characterizations of input-to-state stability. *IEEE Transactions on Automatic Control*, *41*, 1283–1294.
Soo Sim Daniel, N. (2003). Free space optics communication for mobile military platforms. Available in http://calhoun.nps.edu/handle/10945/6160.
Wang, Y., Rajamani, R., & Bevly, D. (2014). Observer design for differentiable Lipschitz nonlinear systems with time-varying parameters. In *53th IEEE conference on decision and control*. Los Angeles, CA, USA.
Zemouche, A., Rajamani, R., Phanomchoeng, G., Boulkroune, B., Rafaralahy, H., & Zasadzinski, M. (2017). Circle criterion-based $\mathcal{H}_\infty$ circle observer design for Lipschitz and monotonic nonlinear systems – enhanced LMI conditions and constructive discussions. *Automatica*, *85*, 412–425.
Zhang, D., N'Doye, I., Ballal, T., Al-Naffouri, T.-Y., Alouini, M.-S., & Laleg-Kirati, T.-M. (2020). Localization and tracking control using hybrid acoustic-optical communication for autonomous underwater vehicles. *IEEE Internet of Things Journal*, *7*(10), 10048–10060.

**Ibrahima N'Doye** is a Research Scientist with the Electrical Engineering Department at King Abdullah University of Science and Technology (KAUST). He jointly received a Ph.D. degree in Automatic Control from the Research Center of Automatic Control, University of Lorraine (CRAN-CNRS), Nancy, France, and a Ph.D. degree in Control Systems and Industrial Informatics from University Hassan II Ain Chock, Casablanca, Morocco, in 2011. He is currently a Research Scientist with the Estimation Modeling and Analysis (EMAN) Group at KAUST. He was a Postdoctoral Researcher with the Faculty of Science, University of Luxembourg, Luxembourg, and the King Abdullah University of Science and Technology. His main research interests are in estimation and control systems engineering. He is a recipient of the IEEE Senior Member grade in 2020. He is currently serving as an Associate Editor for the Proceedings of The Institution of Mechanical Engineers, Part I: Journal of Systems and Control Engineering (JSCE).

**Ding Zhang** received his B.Eng. degree in Mechanical Engineering from Huazhong University of Science and Technology, Wuhan, China, in 2018. From May 2019 to August 2019, he was a research intern at King Abdullah University of Science and Technology, Thuwal, Saudi Arabia. From September 2019 till now, he has been working towards his Ph.D. degree in Electronics and Computer Engineering at Hong Kong University of Science and Technology, Hong Kong SAR. He also works as a research intern at Huawei Hong Kong Research Center since September 2021. His current research focuses on phase analysis, mixed gain-phase analysis of large-scale networked systems, in particular, congestion control protocols in communication networks. In a broader sense, he is interested in fundamental control theory and its application in complex networks, spectral graph theory, and nonlinear observer design.

**Ania Adil** received the M.Sc. degree in applied mathematics from The Mouloud Mammeri University of Tizi-Ouzou, Algeria, in 2018. She is currently pursuing the Ph.D. degree at the same university. She was a Visiting Student with the King Abdullah University of Science and Technology (KAUST), Thuwal, Saudi Arabia, from 2019 to 2021. Her research interests are in the area of estimation and observer design for nonlinear systems.

**Ali Zemouche** received his Ph.D. degree in automatic control in 2007, from the University Louis Pasteur, Strasbourg, France, where he held post-doctorate degree from October 2007 to August 2008. Dr. Zemouche joined, as Associate Professor, the Center de Recherche en Automatique de Nancy at Université de Lorraine, since September 2008. He held an academic position at Inria — Saclay (EPI DISCO) from September 2016 to August 2017. His research activities include nonlinear systems, state observers, observer-based control, time-delay systems, robust control, learning-based methods, and application to real-world models. Dr. Zemouche is currently associate editor in leading international journals: *SIAM Journal of Control and Optimization, IEEE Transactions on Automatic Control, Automatica*, *European Journal of Control*, *and IEEE Systems Journal*. He is also a member of the Conference Editorial Board of IEEE Control Systems Society and IFAC TC2.3 (Non-Linear Control Systems) and has an Erdös number of 3. He has over 55 peer-reviewed journal papers, an edited Springer book, and 10 book chapters.

**Rajesh Rajamani** (Fellow, IEEE) received the B.Tech. degree from the Indian Institute of Technology Madras, Chennai, India, in 1989, and the M.S. and Ph.D. degrees from the University of California, Berkeley, CA, USA, in 1991 and 1993, respectively. He is currently the Benjamin Y.H. Liu-TSI Endowed Professor of Mechanical Engineering and Associate Director (Research) of the Minnesota Robotics Institute, University of Minnesota, Minneapolis, MN, USA. He has coauthored more than 170 journal papers and is a co-inventor on 17 patent applications. He is the author of the popular book *Vehicle Dynamics and Control*published by Springer Verlag. His active research interests include estimation, sensing and control for smart mechanical systems. He was the Chair of the IEEE CSS Technical Committee on Automotive Control and is currently a Senior Editor of the IEEE TRANSACTIONS ON INTELLIGENT TRANSPORTATION SYSTEMS. Dr. Rajamani is a Fellow of IEEE and ASME and was the recipient of the CAREER Award from the National Science Foundation, the Ralph Teetor Award from SAE, the O. Hugo Schuck Award from the American Automatic Control Council, and a number of best paper awards from conferences and journals. Several inventions from his laboratory have been commercialized through start-up ventures co-founded by industry executives. One of these companies, Innotronics, was recently recognized among the 35 Best University Start-Ups of 2016 in a competition conducted by the US National Council of Entrepreneurial Tech Transfer.

**Taous Meriem Laleg-Kirati** is an Associate Professor in the Division of Computer, Electrical and Mathematical Sciences and Engineering (CEMSE) at King Abdullah University of Science and Technology (KAUST). Laleg joined KAUST in 2011 after being a postdoctoral fellow and a researcher at the French Institute for research in Computer Sciences and Control Systems (INRIA) in Bordeaux. She received her Ph.D. in Applied Mathematics in 2008 from INRIA and Versailles University. Laleg's work is in the general area of mathematical control theory, systems modeling, signal processing and their applications. Her primary research goals are directed towards developing effective estimation methods and algorithms to understand complex systems and extract hidden information and design control and monitoring strategies. Her research projects are motivated by applications in engineering and biomedical fields. Laleg was elevated to an IEEE senior member in 2015. She received best paper awards with her students at the IEEE International Conference of the IEEE Engineering in Medicine and Biology Society in 2018 and the IEEE International Conference on Control Engineering and Information Technology in 2015. In 2018, she was among the three finalists in the academic of distinction category (engineering) of the Leadership Excellence for Women Awards (LEWAS). Laleg is member of the IEEE Control Conferences Editorial Board (CEB) and a technical committee member at the International Federation of Automatic Control (IFAC). She is also member of the steering committee of KAUST women in data science.